Pergamon

Journal of Structural Geology, Vol. 17, No. 8, pp. 1165 to 1182, 1995

0191-8141/95 $9.50 + 0.00

0191-8141(95)00001-1

Distinct element modeling of deformation bands in sandstone

MARCO A. ANTONELLINI and DAVID D. POLLARD

Rock Fracture Project and Department of Geological and Environmental Sciences, Stanford University, Stanford, CA 94305-2115, U.S.A.

(*Received* 30 *March* 1994; *accepted in revised form* 14 *December* 1994)

Abstract—We have conducted numerical experiments with the distinct element method to study factors that control the development of deformation bands in sandstone. These experiments show how sorting and initial porosity of the host rock control the development and the mode of deformation in the area of strain localization. The results of the numerical experiments are in qualitative agreement with field and microstructural observations of deformation bands at Arches National Park (Utah).

In our numerical experiments sand grains are modeled as cylindrical elements that move in response to externally applied boundary conditions. Systems of elements that have a large variability in radius and/or loose packing deform at lower applied stresses than systems of elements that have a uniform radius and/or tight packing. The mode of deformation in the first kind of aggregate is particulate flow, where elements of different sizes move easily with respect to each other due to a low degree of interlocking. The mode of deformation in the second kind of aggregates is localized failure on small deformation bands. Shear bands in our numerical experiments nucleate as a zone of dilatancy and propagate via organization of dilatant zones into discrete faults. The presence of a flaw in the form of a 'weak' grain promotes the nucleation and propagation of shear bands.

INTRODUCTION

Faults in sandstone have distinctive characteristics regarding their evolution and microstructure (Aydin 1978, Aydin & Johnson 1983, Antonellini *et al.* 1994). The simplest fault in sandstone is a single small 'fracture-like' structure called a deformation band. Deformation bands are 1–2 mm thick and accommodate small offsets (1 mm–100 mm). Many deformation bands (up to 300–500) form in zones of deformation bands; these zones accommodate offsets of 100 mm up to 10 m. Offset in excess of a few meters is usually associated with the development of a discrete slip plane, a smooth surface where extensive comminution and recrystallization of mineral grains takes place. The slip plane represents a displacement discontinuity in the sandstone body and it usually has well-developed slickensides. In contrast, deformation bands lack a well-defined surface of displacement discontinuity and have characteristics similar to a distributed zone of shearing.

The microstructure of a deformation band, as described by Antonellini *et al.* (1994), is characterized by volume changes and/or grain crushing. Positive dilatancy with little or no grain crushing is usually observed in deformation bands that form in low-porosity (<12%) host rocks at low mean compressional normal stress. Compaction and grain crushing are better developed in deformation bands that form in sandstones with high-porosity (>12%) and high mean compressional normal stress; these deformation bands exhibit well-developed cataclasis (Antonellini *et al.* 1994).

Field observations and microstructural analysis of thin sections from deformation bands in different sandstone types have shown that factors besides porosity and stress state can influence the development of microstructures (Antonellini *et al.* 1994). Sorting of the sand grains, clay content, and mineralogy all play a role in the development of microstructures and in the mechanical behavior of the band. At Arches National Park it is possible to study deformation bands that have formed under similar stress states, but in sandstones with different sorting. If the host rock is well-sorted, grain crushing is well-developed in the deformation bands, whereas almost no grain crushing develops in poorly-sorted sandstone (Antonellini *et al.* 1994).

Deformation bands in poorly sorted sandstones are thinner and accommodate more offset (Fig. 1) than those formed in well-sorted sandstones (Antonellini *et al.* 1994). Large offset (>10 m) fault zones in poorly

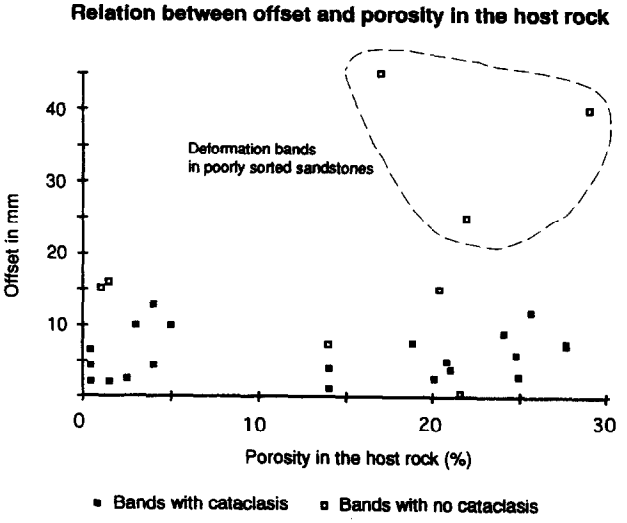

Fig. 1. Relation between offset in the deformation band and porosity in the host rock. Deformation bands with no cataclasis forming in poorly sorted sandstones accommodate more offset than deformation bands with cataclasis that form in well-sorted sandstones.

sorted sandstones and/or in sandstones with high clay content tend to be very localized: the fault-related deformation is restricted to a few decimeters across the fault zone (Antonellini *et al.* 1994). On the other hand, in well-sorted sandstones the fault-related deformation is spread over several tens of meters across the fault zone (Antonellini & Aydin in press). Apparently poor grain sorting in the sandstone promotes localized deformation and inhibits the strain hardening effect observed in high-porosity, well-sorted sandstones (Rudnicki & Rice 1975, Aydin & Johnson 1983, Antonellini *et al.* 1994).

Understanding the factors controlling microstructure development and localization characteristics of deformation bands is important for predicting the petrophysical properties and the distribution of faults in sandstone. Deformation bands and slip surfaces may create a barrier to fluid flow in the direction perpendicular to their plane if their microstructure is associated with porosity reduction and grain crushing. In contrast, deformation bands and slip surfaces may provide a preferential conduit for fluid flow in the direction parallel to their plane because of volume increase in the fault zone due to positive dilatancy or because of the slip-plane discontinuity (Antonellini & Aydin 1994).

The mechanics of an aggregate of particles in contact is complicated and few analytical solutions, under special boundary conditions, are available (Brandt 1955, Deresiewicz 1958). These solutions apply to particles with the same radii arranged in linear arrays (Hara 1935) or in simple cubic, body-centered cubic, and face-centered cubic packings (Duffy & Mindlin 1957, Rowe 1962, Ko & Scott 1967, Maklhouf & Stewart 1967). At present the mechanics of complex particulate aggregates with different grain size distributions can only be studied via numerical modeling and lab experiments. The distinct element method (DEM) provides a tool to investigate the behavior of an aggregate of discrete particles that move and interact with each other during shearing and volumetric deformation within a fault zone. In this paper we present results from numerical experiments performed with the DEM on an idealized granular material made up of cylindrical elements with uniform or different size radii. The elements themselves are not crushed during an experiment. However, the magnitude of the axial stresses resolved by the grains on the boundary blocks and of the contact forces in between elements as a function of sorting and porosity, enable us to determine the potential for grain crushing during shearing and compaction in an idealized deformation band.

THE DISTINCT ELEMENT METHOD

The distinct element method simulates the behavior of a system of discrete elastic blocks under the effect of some specified force or displacement boundary conditions (Cundall 1971). The interaction between the blocks is controlled by their shear and normal stiffnesses and by a friction law at the contacts. The movements of the blocks are calculated at every iteration in the program, and these iterations have a duration determined by a small time step (Δt). Block movements result in forces at their points of contact with neighboring blocks and these can be calculated using a defined force-displacement relationship.

The Distinct Element Method (DEM) was first applied to rock and soil mechanics problems by Cundall (1971). It derives from the Particle Dynamics Method (PDM) extensively used in chemistry and physics (Allen & Tildsley 1987, Gould & Tobochnick 1988) to model liquid and gas behaviors as well as atomic and subatomic particle interactions (Hockney & Eastwood 1989).

Early developments of the DEM were concerned with studying the failure of jointed rock masses (Cundall 1971, Maini *et al.* 1978, Lemos *et al.* 1985). Soon it became apparent that the DEM had potential applications to soil mechanics, specifically in the effort to develop constitutive relations for granular media (Cundall & Strack 1979, Cundall 1987, 1988, 1989). In fact, a granular medium is composed of distinct particles that interact only at contact points; these discrete characteristics of the medium result in a complex behavior during loading of the particulate system.

The problem of shear band localization in an idealized granular material has been investigated with the DEM by Cundall (1989) and by Bardet & Proubet (1992a, b). In these numerical experiments it was observed that the shear band width decreased as the amount of strain in the sample was increased. All the experiments reported in this context have been conducted on systems of elements with the same size or with very similar size (e.g. a ratio of 25/15 between radii of different elements).

Recently, the DEM has been used in sedimentology to study the micromechanics of bedload transport (Jiang & Haff 1993) and to simulate aeolian saltation and mechanical sorting of grains (Haff & Werner 1986, Werner 1987, Anderson & Haff 1988, 1991). Applications of the DEM to faulting in the overburden above reactivated basement normal faults of an extending region have been investigated by Saltzer & Pollard (1992), and a DEM analysis of the boundary conditions used in laboratory sand-box experiments has been presented by Saltzer (1993).

A description of the force-displacement laws and of the equations of motion implemented in our DEM code is given in the appendix. Further details on the formulation of the distinct element code and comparison with existing codes such as BALL, TRUBAL (Cundall & Strack 1979, Strack & Cundall 1984) and DEC (Saltzer 1992) are presented in Antonellini (1994).

EXPERIMENTS

Boundary conditions

To investigate the microstructure of deformation bands we study a small volume of granular material (Fig. 2) that is deformed in a numerical 'testing machine' (Fig. 3a). At this point in the study of defor-

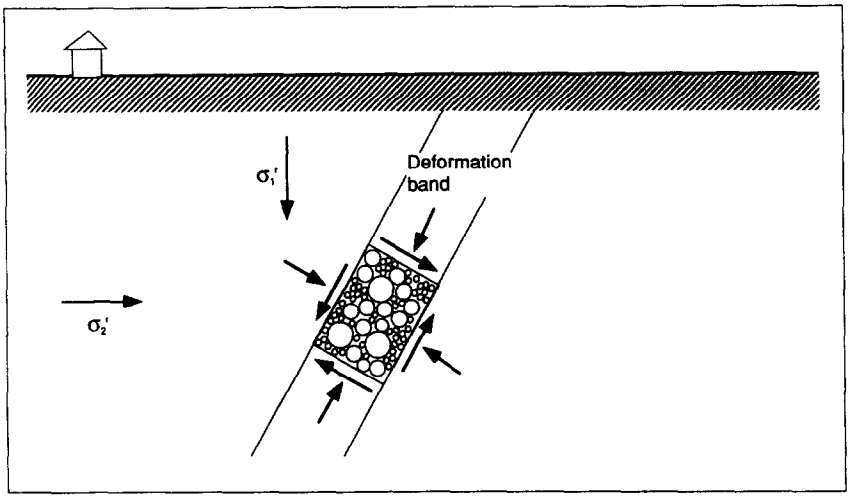

Fig. 2. Boundary conditions in a deformation band. Under remote stress state conditions (σ_1', σ_2') deformation localizes in a narrow band across which some shear offset occurs. Normal and shear tractions are applied at the boundaries of a small volume of material in the deformation band.

mation bands we are not concerned with the problem of localization of deformation into a narrow zone (shear band) but only with the factors that control the stresses acting on the band, and the development of the microstructure within the band.

The boundary conditions on the idealized deformation band and the experimental set up are presented in Figs. 2 and 3(a). In the figures presenting the results of the experiments we use a simplified representation of the testing machine which is shown in Fig. 3(b). Under remotely applied stresses (σ_1', σ_2') the grains along the boundaries of a small volume of granular material within the area of shear localization are subject to a complex distribution of normal and shear tractions. To approximate these boundary conditions in the DEM, we confine the volume of granular material with four rectangular rigid blocks that can move with a specified velocity (Figs. 3a and 5b). These bounding blocks are designed to impart the average tractions from the complex distribution of actual tractions to the grains they contact.

The bounding blocks can be used to impart either a velocity boundary condition or a traction boundary condition (Fig. 3b). In both cases a boundary velocity is specified. The bounding blocks are analogous to the actuators of a servo-controlled testing machine (Fig. 3a). The traction boundary conditions are imposed by controlling when and in what direction the blocks move. They move at a constant velocity toward the interior of the sample if the average normal traction resolved by the grains on the block is less compressive than the prescribed traction, whereas they move at a constant velocity away from the center of the sample if the average normal traction resolved by the grains on the block is more compressive than the prescribed stress.

An experiment is performed on the granular aggregate by moving the top and bottom blocks along the y axis and the lateral blocks along the x axis. If the top and bottom blocks also move along the x axis as shown in Fig. 3(b), it is possible to impose shearing in addition to biaxial loading. We hypothesize that such loading simulates on a first approximation the boundary conditions that control the formation of microstructures within deformation bands.

The displacement of the blocks can be controlled to simulate different degrees of confinement on the granular material (corresponding to different confining pressures). The stresses developing in the granular aggregate are a function of the displacements only, not of the rate (velocity) at which they are applied. During movement the boundary blocks do not interfere with one another (Fig. 3a), because the two lateral blocks are shortened at the same rate the top and bottom blocks approach each other. Using purely velocity boundary conditions one can control the movements of the walls and therefore control the bulk volumetric strain. Experiments with uniform grain sizes and regular packing have been done using both kinds of boundary conditions. Experiments with different grain size distributions have been done using only velocity boundary conditions.

Sample preparation

Two methods of element generation are employed. The first generates regular packings of elements within the volume, and is used when the system is made up of elements with the same radius. The second method is based on a random particle generator and is employed to study the behavior of a system of elements with very different radii. In this latter case any set of elements corresponding to the desired grain size distribution can be generated in the volume. A random number generator produces the coordinates of the elements centroid; first the large grains are created and then small grains in order of decreasing diameter (Fig. 4a). If an element overlaps another one it is discarded. The random number generator tries to fit an element in the voids left at any given instant in time, repeating this operation until a satisfactory number of elements is available. It is poss-

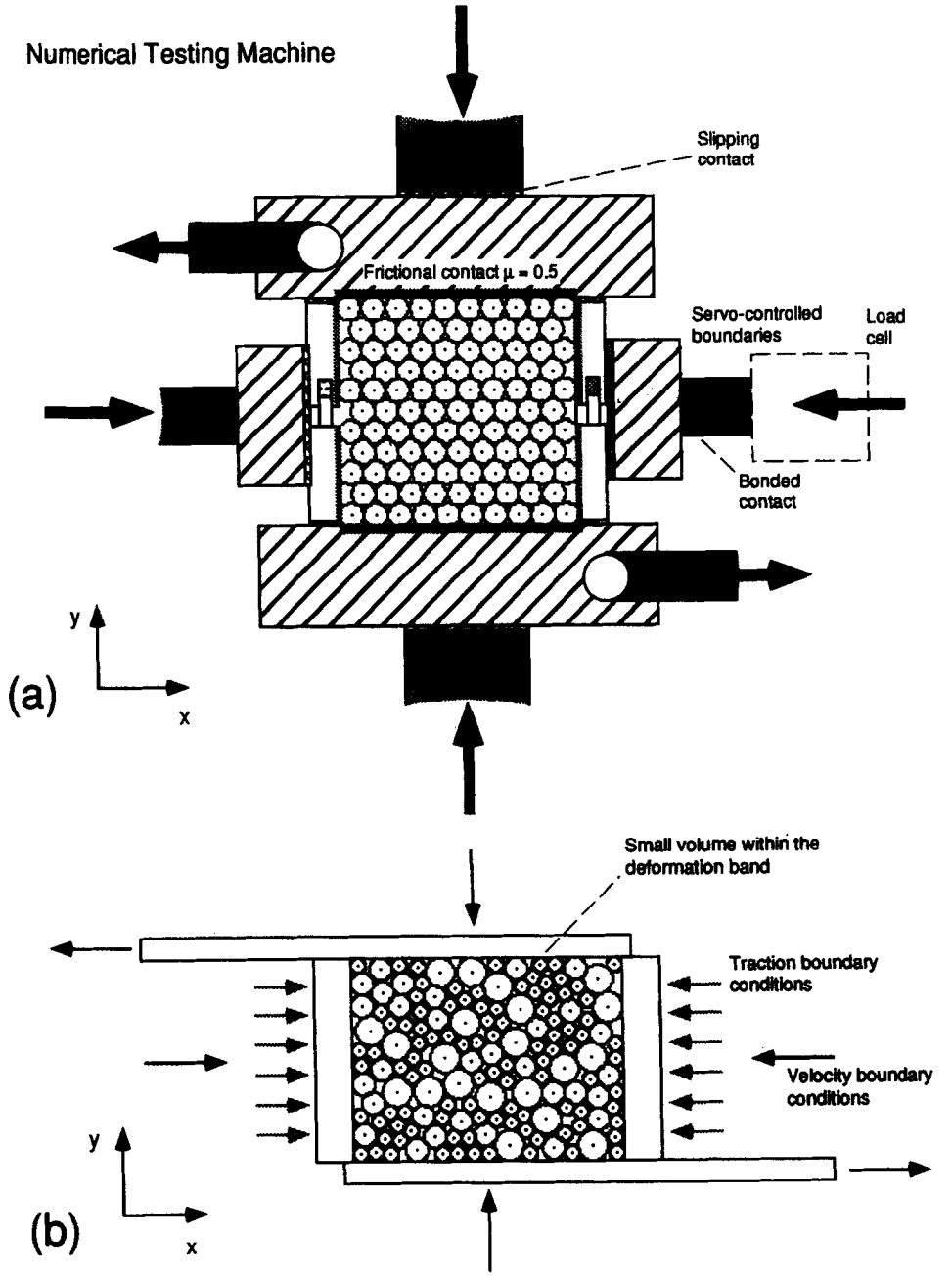

Fig. 3. (a) Idealization of the experimental set up for the numerical testing machine that has been used to make experiments on the granular media discussed in this paper. Normal and shearing velocity boundary conditions can be applied to the top and bottom plates, whereas normal velocity or servo-controlled stress boundary conditions can be applied to the lateral walls of the testing machine. The lateral walls can deform without interfering with the top and bottom plates. (b) Simplified representation of the testing machine and of the boundary conditions used in the figures of this paper.

ible to avoid a bias in element distribution by using a large volume to generate the elements.

After the granular material has been generated it is compacted to a prescribed porosity before the experiment. To achieve the desired compaction, the four walls of the testing machine are moved toward the interior of the sample at an equal constant velocity. Once the granular aggregate has reached the required porosity the walls of the testing machine are stopped and the sample is left to stabilize for about 1000 iterations (Fig. 4b). After compaction and stabilization an experiment is performed by moving the boundary walls according to the specified boundary conditions.

The results of an experiment can be viewed by watching the positions of the elements at a given snapshot in time and/or by analyzing the average tractions resolved on the boundary plates. For example, the stress on the top plate of the testing machine (axial stress) can be plotted vs the axial strain. The analysis of this curve in conjunction with the observation of the element positions at a given time provide insights into the contact forces arising between the elements and on the average stresses within the granular aggregate. The effect of the development of specific structures on the average stresses in the granular aggregate can therefore be monitored during the experiment.

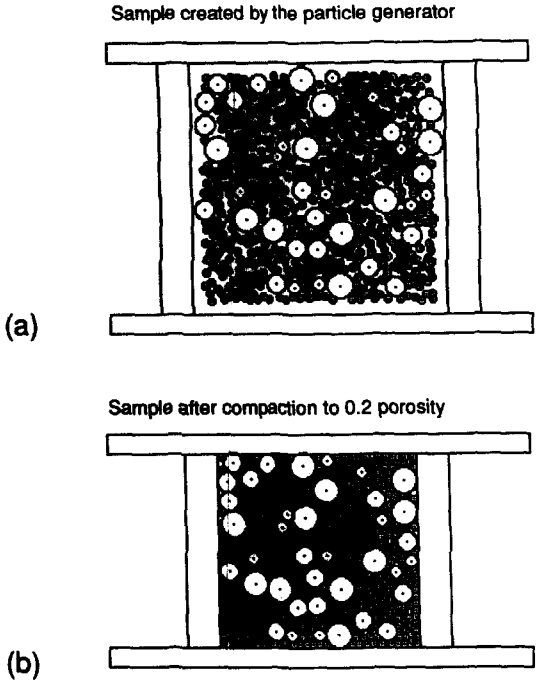

Fig. 4. Preparation of a sample with elements of different sizes. (a) Elements are generated randomly according to a specified grain size distribution within the volume of the testing machine. (b) The sample is compacted at the porosity desired for the experiment that we want to make.

Experiments with uniform grain size

One hundred and five elements arranged in regular hexagonal packing, or in alternate layers of cubic and hexagonal packing, were generated within the volume of the testing machine (Fig. 3a). The elements have a radius of 4 mm, a density of 2800 kg m^{-3} and a length of 25 mm. To simulate a geologic material we use a Young's modulus E = 95.3 GPa (typical for quartz; Zhang *et al.* 1990) and a Poisson modulus ν = 0.25. The coefficient of sliding friction, μ, is set to 0.5.

The first set of experiments were conducted in the biaxial configuration without a shear velocity at the top and bottom plates of the testing machine. Two element configurations have been considered. In the first the elements were arranged in a closest hexagonal packing with a porosity of 0.153. In the second the elements were arranged in rows with cubic packing (4 rows) sandwiched between elements arranged in hexagonal packing (8 rows); the initial porosity of the aggregate was 0.22.

The velocity of the upper plate in the y direction was set to 0.01 mm per time increment (Δt = 0.05423 s); the lateral walls moved at a velocity that allows the sample to deform with a small volumetric strain; typically after 10,000 iterations the volumetric strain of the sample is less than +0.02, while the axial strain is −0.14. The velocity of the lateral walls is arbitrary and it is chosen to simulate the amount of volumetric strain usually observed in lab experiments on soil samples (Wood 1990). If we impose a deformation with zero or negative volumetric strain, the axial stresses during an experiment increase steeply because of the large interpenetrations between neighboring elements. If the interpenetrations become too large the experiment may become unstable. Physically, large interpenetrations correspond to large contact forces which would cause the crushing of the elements in the sample.

Figure 5 shows the evolution of the vertical stress resolved by the elements on the upper plate of the testing machine with time. In the high-porosity sample (Fig. 5a) the stress increases steeply at the beginning of the experiment as the elements react to the movement of the plates (stage 1). After this initial stage, the curve flattens (stage 2) and after the axial strain has reached a value of −0.08 the granular medium softens producing a decrease in the stress on the plate. Observations of the element positions demonstrate this. Stage 1 represents the destruction of the skeleton of contacts in the cubic packing and stage 2 is characterized by the movement of grains by a particulate flow mechanism. Particulate flow is a discontinuous deformation mechanism that involves grain sliding and rotation (Borradaile 1981). In our experiments we observe that this mechanism allows grains to slip and roll past one another by creating local disorganized areas of dilatancy. Particulate flow results in a distributed intergranular deformation that does not localize in any specific area of the sample. Particulate flow has been experimentally observed in Berea Sandstone deformed at low effective stresses (Handin *et al.* 1963). It is also commonly observed in sediment–fluid mixtures (Lasek 1992).

The same experiment performed on a regular tight hexagonal packing of circular elements produces a much different result (Fig. 5b). The stress on the top plate increases with a relatively steep gradient from 0 to −0.07 axial strains (stage 1), then the curve flattens out and the stress decreases gradually until −0.12 axial strain (stage 2), after which the stress increases again in a relatively steep fashion (stage 3).

In the stress–strain curves, the steeper segments correspond to the growth of shear bands in the granular aggregate (Figs. 6a and c) and the consequent increase in stresses due to the dilatation in the band as the elements slide past each other. The flatter or shallower slope segments of the stress–strain curve correspond to the destruction of porosity in the shear band and the subsequent rearrangement of the elements into a tighter hexagonal packing (Fig. 6b). The stress does not go back to zero after destruction of the dilatancy in the first set of shear bands, because the impact damping scheme employed imposes a linear gain in energy of the elements during the experiment. It is also apparent by the change in scale of the diagrams that the magnitude of the stress during the second experiment (Fig. 5b) is 10–100 times larger than in the first (Fig. 5a). These observations indicate that it is easier to cause grain movement in a high-porosity sample than in a low-porosity one. In the first sample the grains arranged in a cubic packing move by sliding away from their initial contact points to the sides without finding any obstacle; this causes compaction and porosity reduction. In the second sample the grains arranged in an hexagonal packing move by climb-

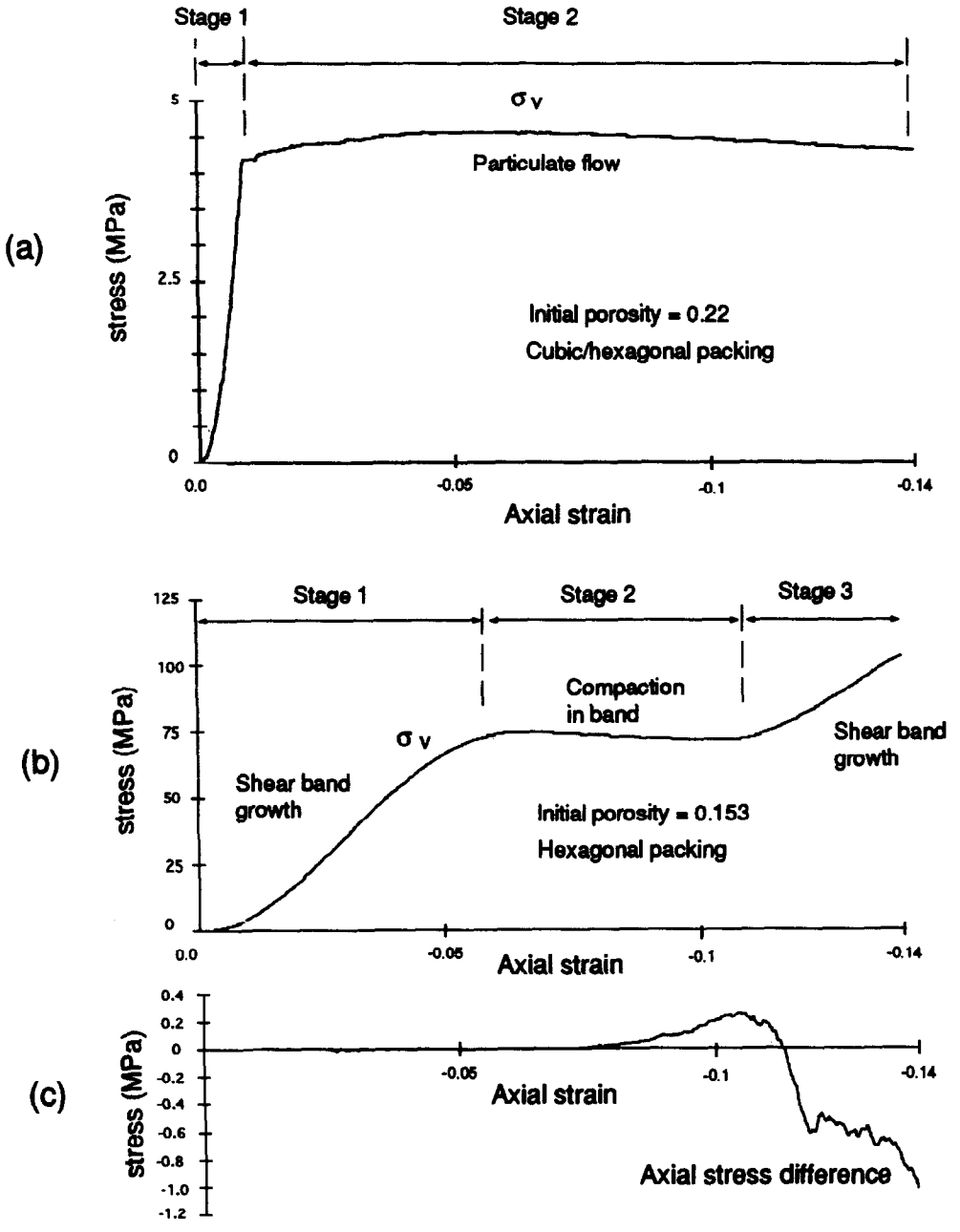

Fig. 5. Biaxial test on the granular aggregate. (a) Vertical stress on the top plate of the testing machine in an high-porosity granular medium (porosity = 0.22) with uniform grain size distribution. (b) Vertical stress on the top plate of the testing machine in a low-porosity granular medium (porosity = 0.153). (c) Axial stress difference between the experiment with shear at the top and bottom walls and the experiment with no shear (Fig. 6b).

ing up on the neighboring grains, thereby increasing locally the porosity within a zone that develops into a shear band; this porosity increase causes large contact forces resulting in larger average tractions on the boundary blocks.

To simulate the boundary conditions within a deformation band in a well-sorted sandstone arranged in a tight hexagonal packing, a shear velocity ($v = 0.05$ mm Δt^{-1}) was imparted to the top and bottom walls of the testing machine together with the already mentioned normal velocities. The result of the experiment (Fig. 7) shows that the shear on the boundary walls does not cause many changes in the style of deformation. As demonstrated in Fig. 7, two shear bands are well-developed at an axial strain of -0.028 (Fig. 7b), at an axial strain of -0.056 the porosity in the band starts to be destroyed (Fig. 7c), and at an axial strain of -0.084 the shear bands have disappeared. In this experimental set up the shear at the walls has no influence on where and when the shear bands form in the granular system. The stress difference between the experiment with shear velocity at the top and bottom walls and the experiment with no shear velocity is on the order of 1% of the total stress (Fig. 5c).

Experiments with different grain size distributions

One of the objectives of our project was to study the effect of sorting of particles on the mechanical behavior of the granular system subjected to simple loading histories. This investigation can provide insights on the bulk behavior of a sandstone and on the specific behav-

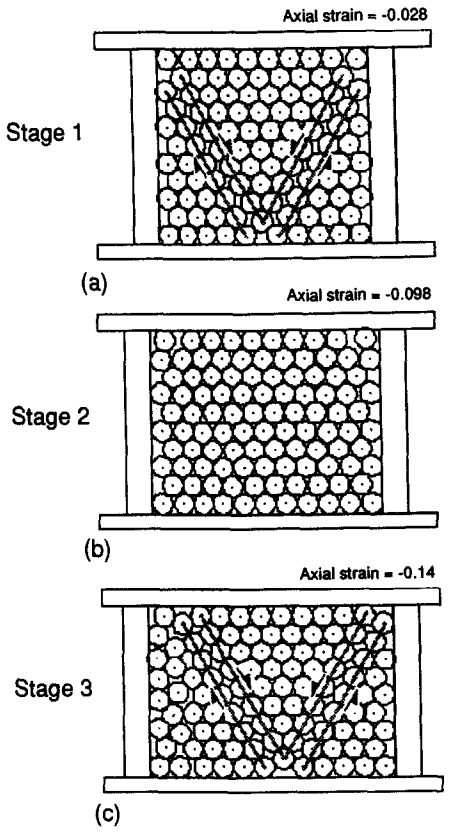

Fig. 6. Biaxial experiment on a sample of uniform radii elements. The deformation is accommodated by the localization of dilatant shear bands (confined in between the shaded lines) that are subsequently compacted. The sense of shear is indicated by the arrows. (a) Dilatant shear bands form to accommodate the deformation. (b) The dilatation in the shear bands disappear as the sample is compacted. (c) More shear bands form to accommodate further deformation.

ior of the gouge material in a deformation band. Fragmentation processes in fault zones, in fact, cause grain size reduction and the development of poorly sorted grain size distributions (Turcotte 1992). Our results clearly are relevant to the study of small faults and they also may be relevant to the study of more complex fault zones.

Before describing the experiments in detail, it is necessary to quantify some parameters that allow us to compare different grain size distributions. Poorly sorted sediments are usually associated with catastrophic mass transport events and/or with diagenetic and mechanical processes that change the grain size distribution via mineral alteration and/or mechanical breakage of the grains. In this study we restrict ourselves to the particle size distributions that have been generated by fragmentation and diagenesis, because a framework in which to compare them is available (e.g. Blenkinsop 1991).

Extensive work has been done in documenting and measuring grain size distributions in the gouge material of fault zones (Biegel *et al.* 1989, Marone & Scholz 1989, Sammis & Biegel 1989, Blenkinsop 1991). Blenkinsop (1991) has documented that power-law distributions can approximate the observed grain-size distributions produced by diagenetic and fragmentation processes between limits of 0.3 and 0.03 mm (these limits are called the upper and lower fractal limits by Blenkinsop 1991). Sammis & Biegel (1989) argue that such distributions can be characterized by a dimension (or exponent), D, expressed as

$$D = \frac{\ln[N(n)/A]}{\ln[1/L(n)]} \quad (1)$$

where $N(n)/A$ is the number of particles of class n per unit area (or volume if considering a three-dimensional case), and $L(n)$ is the average diameter of the particles in class n. A *class* is a set of particles with very similar size. A $D = 2.5$–2.6 corresponds to the self-similar (fractal) grain size distribution of Sammis & Biegel (1989).

Shear tests on artifical gouges of Ottawa sand and Westerly granite (Biegel *et al.* 1989, Marone & Scholz 1989) have shown that grain crushing and comminution produce particle-size distributions with $D = 2.58$–2.6. A similar grain-size distribution ($D = 2.6$) has been documented in the Lopez fault zone of the San Gabriel Mountains in California (Sammis *et al.* 1987). Marone & Scholz (1989) and Blenkinsop (1991) have noticed that with high confining pressures D tends to increase ($D > 2.6$), which corresponds to the disappearance of the largest particles from the grain-size distribution, a phenomenon that has also been qualitatively observed by Engelder (1974). On the other hand, weathering and diagenesis (Blenkinsop 1991) tend to produce grain size distributions with smaller D ($D < 2.6$).

Samples with power-law grain-size distributions (Fig. 8), characterized by a D between 0.88 and 5.0 and a radius between 1 and 4 mm, were generated using equation (1) and compacted to initial porosities of 0.2 and 0.153. The range in D we investigated corresponds to that observed and documented by Blenkinsop (1991). We also used a uniform size distribution of grains with large radius (4 mm) to study the effect of grain size. All samples had the same mass. The experiments were done with a procedure similar to that of the experiments with a regular packing but with a smaller time step ($\Delta t = 0.027$ s).

We monitored the stresses during compaction of the aggregates to 0.2 and 0.153 porosity. The desired compaction with the lowest stress in the sample is achieved with a grain size distribution corresponding to $D = 2.5$ (Figs. 9a and b). Overall grain size distributions skewed towards small grain sizes are easier to compact than grain size distributions with large grain sizes. However, it seems that only the distribution with $D = 2.5$ has the elements in the right proportion to require the minimum amount of energy needed to achieve the desired compaction.

First we describe a set of experiments after initial compaction to 0.2 porosity. Figures 10(a) & (c) represent experiments with no shear velocity and Fig. 10(b) shows the stress difference between the experiments with a shear velocity at the top and bottom plates of the testing machine and those with no shear velocity. The peak stress is greatest in experiments with a uniform grain size distribution of large particles and is less (factor ~8) for the size distribution with $D = 0.88$ (Fig. 10a). The peak stress in these experiments tends to decrease

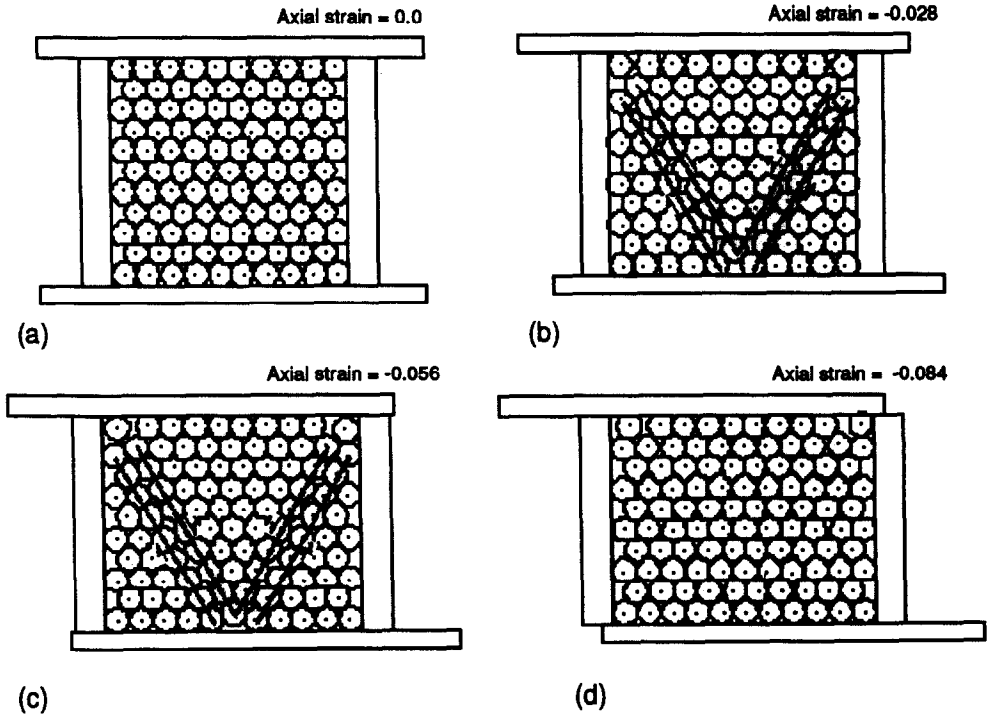

Fig. 7. Deformation band simulation. Shaded lines bound the shear bands forming in the aggregate; the arrows give the sense of shear. (a) Sample in initial conditions. (b) At an axial strain of −0.028 the shear bands are in their dilatant stage. (c) At an axial strain of −0.056 the shear bands are in their compacting stage. (d) At an axial strain of −0.084 no very well-defined shear band is present.

as the exponent of the distribution increases except for distributions with $D > 2.5$. This observation indicates that sorting is important in controlling the stresses during deformation.

A secondary factor also controlling the stresses is the element size. The aggregates with $D > 2.5$ have small elements that are almost uniform (well-sorted). The subordinate dependency of the stress on element size is surprising and will be discussed later.

The curves in Figs. 10(a) & (c) do not show the steps and plateaus present in those experiments where a shear band localizes in the granular aggregate (Fig. 5b). An exception is represented by the uniform distribution in Fig. 10(a); the stress–strain curve for this distribution shows subordinate steps corresponding to the appearance of disorganized shear bands in the sample. In the models compacted to 0.2 porosity the stresses exhibit an initial increase, and tend to level out as the elements deform with a bulk flow mechanism. By watching snapshots of the experiments at different intervals it is clear that well-developed shear bands do not develop, but deformation is accommodated more or less uniformly across the sample. We call this style of deformation particulate flow, because the particles slide and roll past one another with no apparent order ('independent particulate flow' of Borradaile 1981). The difference in the stress history (difference in axial stresses) between experiments with and without shearing is on the order of 20–30% of the total stress for the uniform grain size distribution and less than 10% for the poorly sorted distributions.

Another set of experiments has been conducted after an initial compaction of the samples to 0.153 porosity; for brevity only some selected results are presented here. Figures 11(a) & (c) show the results of the experiments for the case with no shear at the walls and Fig. 11(b) shows the stress difference between experiments with and without shear at the walls. The stress–strain curve for the sample with a uniform grain size distribution illustrated in Fig. 11(a) shows several breaks in slope (labeled 'sb') that are better organized than those in Fig. 11(a). Examination of the element positions at the time of these changes in slope indicates that they are associated with the growth of shear bands and the subsequent collapse of the pore space created by dilatancy. In the experiment with no shear at the walls (Fig. 11a) three episodes of shear band localization take place before the strains reach a value of −0.14. The breaks in slope marking the end of shear band growth are not evident in the power law distributions. These observations indicate that a large initial compaction (i.e. lower initial porosity; 0.153 compared to 0.2) promotes localized deformation in granular aggregates with uniform grain size distribution.

The magnitude of the stresses of these experiments is approximately 100 times larger than in experiments with samples compacted to 0.2 porosity. A significant difference in the stress–strain history between experiments with and without shearing is present only for the case of the uniform size distribution and for the power law distribution with $D = 0.88$ (order 10% of the total stress). In the experiment on the sample with $D = 2.5$ the stresses have the lowest value. Samples with larger exponents ($D > 2.5$) deform at larger stresses probably because the grains become more and more uniform in size.

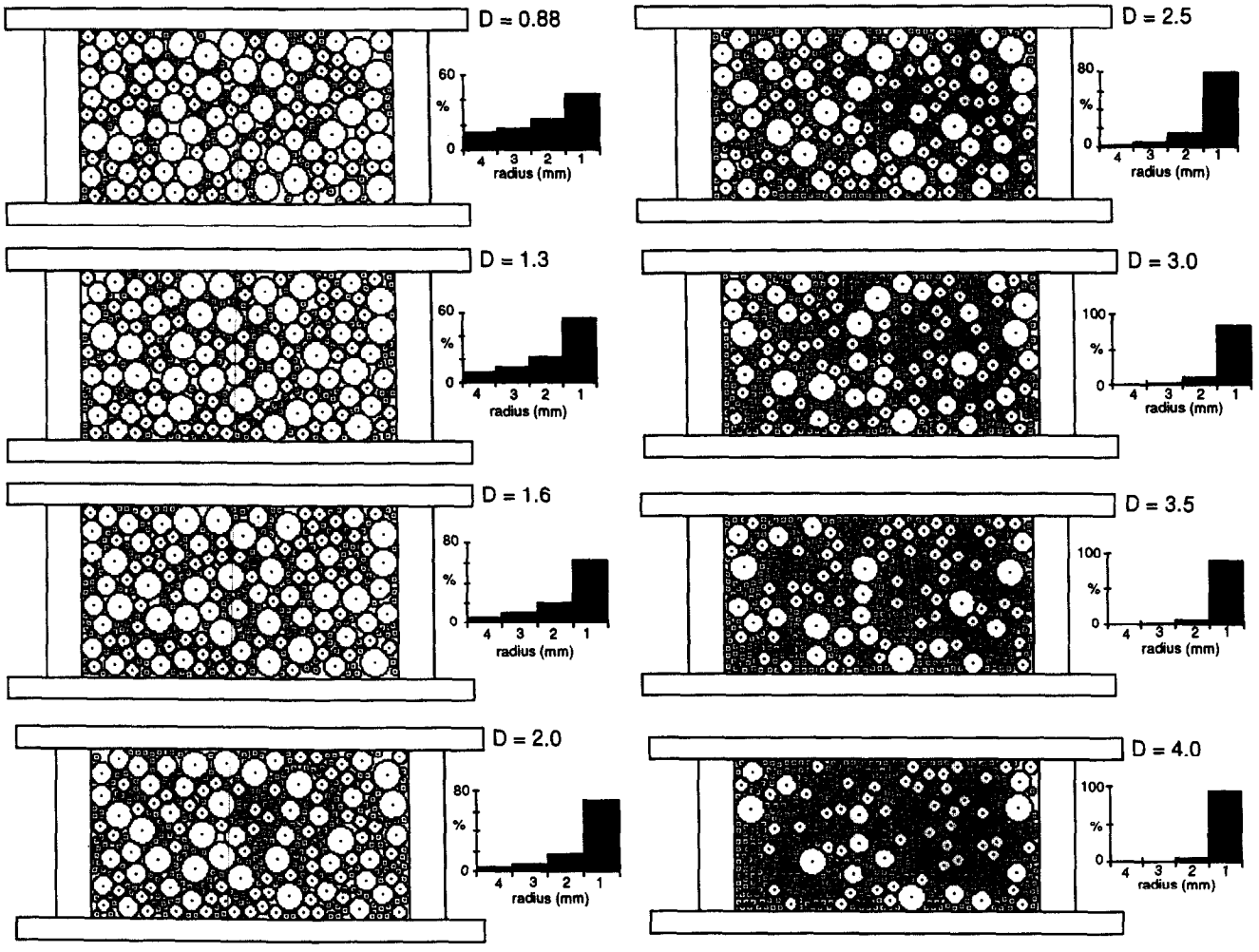

Fig. 8. Samples with different power law grain size distributions tested in biaxial experiments and in the numerical set up to simulate deformation bands boundary conditions. The samples are represented after 50,000 iterations. The grain size distributions are given by the histograms; the exponent of the distribution varies from 0.88 to 4.0.

Poorly sorted distributions, corresponding to $0.88 < D < 3.0$, tend to promote deformation of the particles by a bulk flow mechanism (particulate flow) rather than by shear bands localization at both levels of initial compaction.

Nucleation and growth of a shear band

Here we examine in detail the kinematics of movement of the cylindrical elements that lead to the development of the shear bands shown in Fig. 6(a). These observations provide important insights for the process of deformation band localization in nature.

We look at snapshots of the experiment at the very early stage of shear band growth and at short intervals in time after that (~ every 100 iterations). At an axial strain of −0.02 (Fig. 12a) no shear band has developed. However, at this time four potential nucleation sites, represented by areas of dilatancy (black highlight), have formed. At an axial strain of −0.021 (Fig. 12b) the first development of two organized zones of dilatancy is observed. These zones initiate from the two central nucleation sites and propagate along a surface oriented at 30° to the direction of maximum shortening. The two shear bands grow quickly and at an axial strain of −0.022 (Fig. 12c) they have propagated almost completely through the sample (Fig. 12d).

The presence of 'weak' grains can also trigger the nucleation and subsequent growth of shear bands in granular media. A weak grain is one that, because of its physical properties (e.g. cleavage, grain boundaries, fractures, etc.), can fail under smaller applied loads than the surrounding grains. We examine the influence of a weak grain on shear band localization with a biaxial numerical experiment. In this experiment the critical contact force for that particular grain is reached at an axial strain of −0.011. When the critical contact force is exceeded the grain is crushed and we substitute four smaller cylindrical elements for the original grain (Fig. 13a). The sum of the volumes of the four smaller distinct elements is set at about 70% of the volume of the original grain. This does not represent a loss of mass, rather by decreasing the total volume one can simulate the loss of load bearing capability of the crushed grain. We imagine that 30% of this grain is comminuted into much smaller fragments that fill voids, but do not play any significant role in the forces transmitted through the aggregate. Soon after collapse of the central grain four shear bands develop and propagate from the boundary plates towards the crushed grain (Figs. 13b & c) in a few

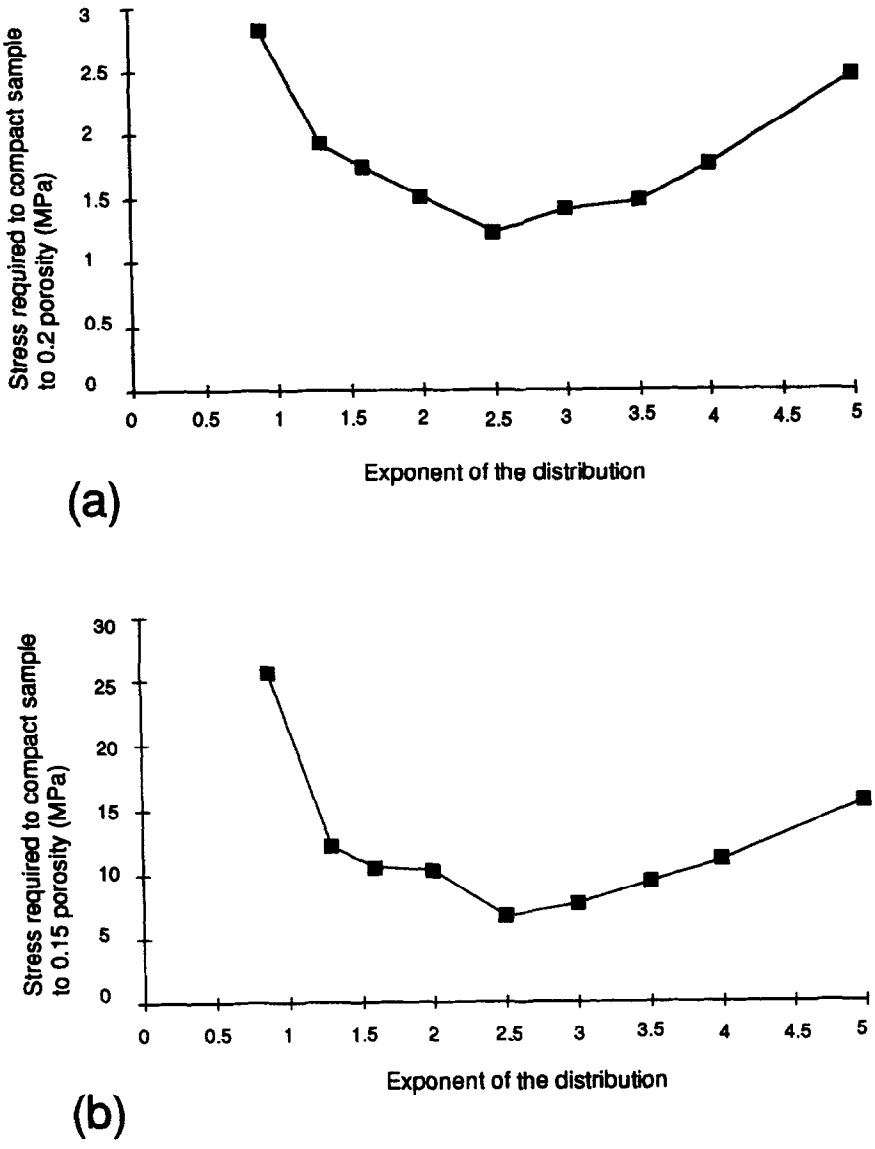

Fig. 9. Maximum applied stress required to compact samples with different grain size distributions to a porosity of 0.2 (a) and 0.153 (b). The grain size distribution which is easier to compact has an exponent $D = 2.5$.

tens of iterations. The localization of shear bands starts just after an axial strain of −0.014, whereas, in the sample without a weak grain, localization of shear bands starts after an axial strain of −0.021 has been reached.

This experiment illustrates the effect of the testing machine boundaries in controlling the nucleating positions of the shear bands. The movement of the rigid boundary blocks induces large contact forces in their proximity, and these forces control the nucleation of shear bands at the boundaries. However, in nature, it is more likely that the crushed grain itself is the nucleating position of the shear bands.

The collapse of a 'weak' grain controls the time at which shear bands localize in the sample, but not necessarily their nucleating position. To further investigate the effect of 'weak' grains on the localization and distribution of deformation bands we have devised an experiment with the 'weak' grain shifted two elements to the right from the center of the sample (Fig. 14a). After grain failure (at an axial strain of −0.011), shear bands localize in the sample (between −0.012 and −0.014 axial strains) with a pattern that is similar to that illustrated in Fig. 13(b). Four shear bands grow toward the crushed grain (Fig. 14b); they are shifted to the right with respect to the center of the sample. In this experiment two additional shear bands develop in the left portion of the sample (Fig. 14b). From the results of this experiment it appears that once the 'weak' grain has collapsed, strain is accommodated via shear bands in zones not in close proximity to the crushed grain. As the experiment proceeds some of the initial shear bands are abandoned and two of them develop more fully in the aggregate (Fig. 14c).

DISCUSSION AND CONCLUSIONS

The DEM experiments on samples with poor sorting demonstrate that deformation via bulk flow occurs at relatively low stresses in the granular aggregate, which result in small forces at grains contacts unlikely to cause grain crushing. These numerical results compare well with the observation that, in poorly sorted sandstones, deformation bands do not show well-developed grain

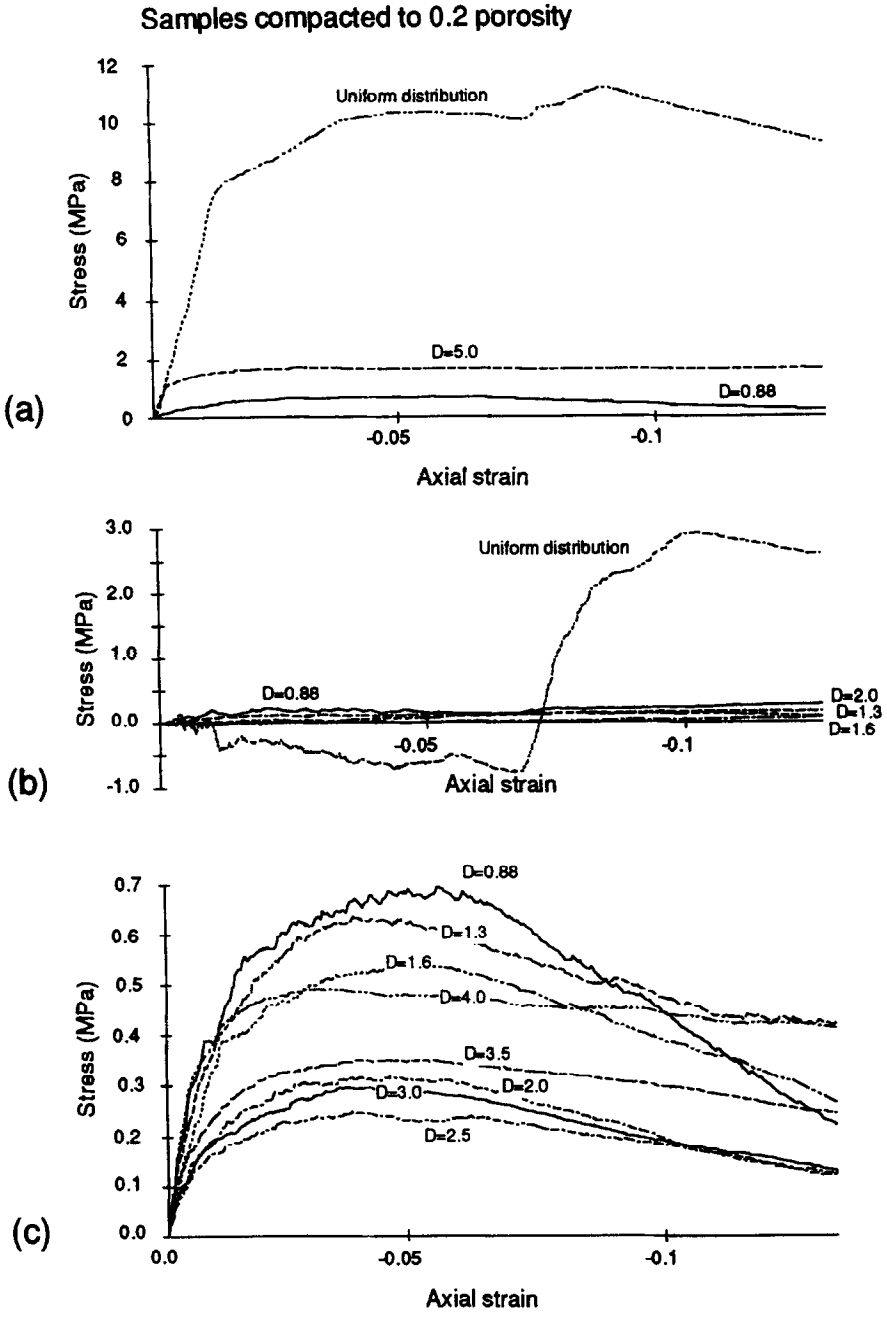

Fig. 10. (a) Biaxial experiments. Vertical stress on the top plate of the testing machine. Samples compacted to 0.2 porosity. (b) Axial stress difference between an experiment with shearing velocity at the top and bottom walls and the experiment in (a). (c) Biaxial experiments on samples with large exponents power law distributions ($D > 2.5$).

crushing and are usually associated with larger offsets (Fig. 1) compared to deformation bands in well-sorted sandstone (Antonellini *et al.* 1994). According to Lambe & Whitman (1969) poorly sorted soils have a lower degree of interlocking among grains than well-sorted soils. They also argue that the degree of interlocking controls how easily a granular aggregate can fail in shear. We suggest that grains deforming via particulate flow in a deformation band within poorly sorted sandstone can accommodate more offset because of the lower degree of interlocking among the grains.

The results of the DEM experiments indicate that the stresses during deformation of a granular aggregate are controlled by the competition of two factors: (1) the grain-size distribution (uniform vs unsorted); and (2) the size of the grains (the larger the grains, the larger the stresses). The second factor is subordinate in respect to the first one. Grain-size distributions skewed towards small grain sizes ($D = 2.5$–3.5) but not completely made up by small grains require the minimum amount of energy during deformation. In the case of hydrostatic compaction this 'minimum energy configuration' is represented by the grain size distribution with $D = 2.5$. In the case of biaxial experiments the 'minimum energy configuration' is represented by grain-size distributions with $D = 2.5$ for samples initially compacted to 0.2 porosity, and with $D = 2.5$–3.0 for samples initially compacted to 0.153 porosity. The latter value is very

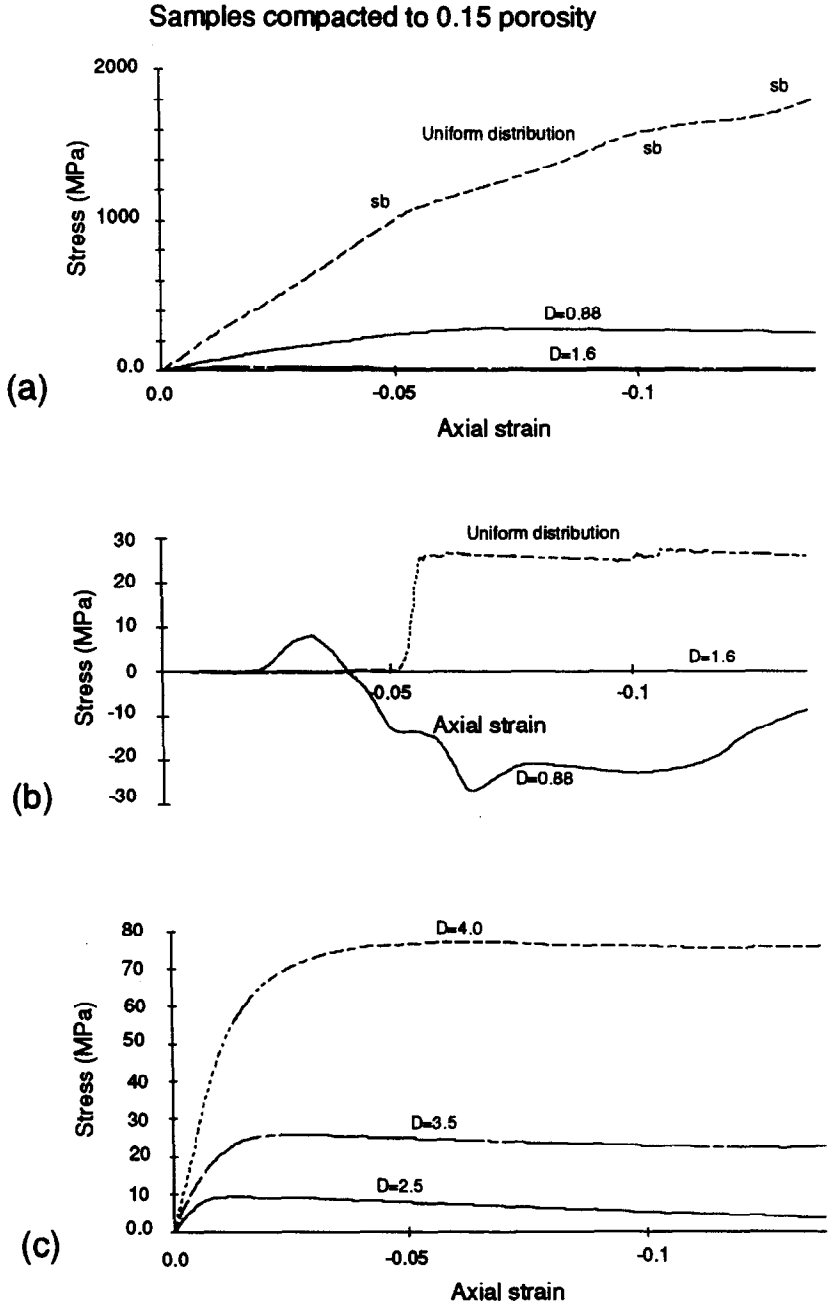

Fig. 11. (a) Biaxial experiment. Vertical stress on the top plate of the testing machine. Samples compacted to 0.153 porosity. 'sb' is the abbreviation for shear band. (b) Stress difference between an experiment with shearing velocity at the top and bottom walls and the experiment in (a). (c) Biaxial experiments on samples with large exponent D.

similar to that measured in fault gouges in both experiments (Biegel & Sammis 1989, Marone & Scholz 1989) and in outcrop (Sammis *et al.* 1987).

The dependency of the stress on element size is surprising, because one would expect a self-similar behavior for elements with large and small radius if the element distributions are uniform. Our numerical experiments, however, are in agreement with lab experiments on glass bead samples by Yin *et al.* (1993) and on sandstone samples by Zhang *et al.* (1990). In particular Yin *et al.* (1993) have observed that large grain size samples have consistently higher P and S wave velocities in respect to small grain size samples and, during loading, they have high levels of acoustic emissions associated with grain crushing. Grain crushing, on the other hand, is not observed in small grain size samples. A grain size effect has also been observed in the microstructure of deformation bands within siltstones of the Dewey Bridge member of the Entrada Sandstone at Arches National Park. The deformation bands in this fine-grained rock do not show any sign of cataclasis. We think that the element size dependency that we observe in the numerical experiments is related to the displacement boundary conditions employed, to the size of the elements relative to the size of the sample, and to the smaller contact forces that arise in a sample with smaller grains because of the partition of the load on a larger number of contact points respect to a sample with large grains.

The effect of porosity on the mode of deformation is

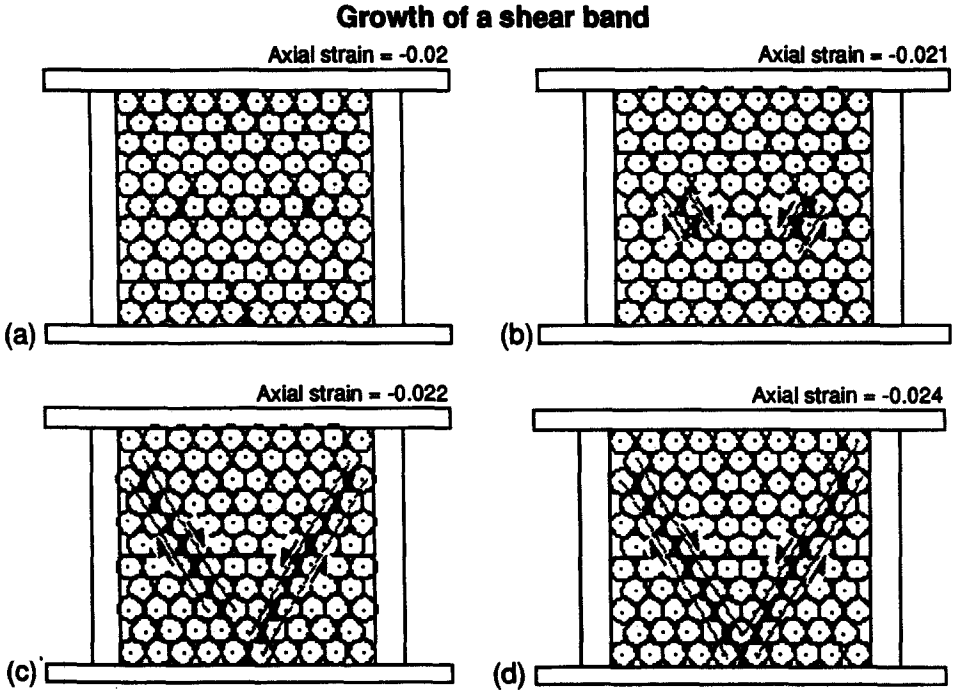

Fig. 12. Growth of a shear band. Dilatancy in black. Shear bands are individuated by the shaded lines. The arrows indicate the sense of shear. (a) At an axial strain of −0.02 iterations the shear bands are not developed, there are four areas of increased porosity. (b) Two shear bands nucleate at an axial strain of −0.021. (c) The two shear bands quickly propagate through the sample. (d) At an axial strain of −0.024 the shear bands have completely propagated through the sample.

also important. A uniform grain size sample compacted to 0.2 porosity exhibits flow instead of localization during biaxial deformation; in fact, the stress–strain curves of the experiments performed on these samples (Fig. 10) do not show the characteristic 'step-like' geometry that is present in some of the experiments conducted on samples compacted to 0.15 porosity (Fig. 11a) and on the samples with a regular packing (Fig. 5b). Dunn *et al.* (1973), Hirth & Tullis (1989), Bernabe & Brace (1990), and Rutter & Hadizadeh (1991) have shown in laboratory experiments on sandstone samples that high porosities cause the deformation to remain distributed, and in the form of cataclastic flow. Low-porosity sandstones, on the other hand, fail by localization and strain softening (Hirth & Tullis 1989). Our numerical experiments are consistent with these laboratory results.

Deformation via localization of shear bands represents a discontinuous deformation that is apparent by the staircase geometry in the stress–strain curve. The localization of a shear band causes the deformation of the sample to proceed in steps (Fig. 5b): during each step the stress first increases steeply ('dilatational stage' of shear band growth) and then it decreases or stabilizes ('compaction stage' of shear band growth). The deformation in the sample is therefore non-uniform. Provided a criterion for grain failure is met, it is likely that grain crushing occurs during the maximum dilatational stage of shear band growth when the contact points among grains in a shear band are relatively few and the contact forces are relatively high. The actual mechanism of grain crushing is via opening mode cracks that start at contact points and propagate through the grain (Aydin 1978).

It is commonly observed in high-porosity sandstones (Aydin 1978, Aydin & Johnson 1983, Antonellini *et al.* 1994) that, after localization of a deformation band accompanied by grain crushing and compaction, further offset is accommodated by localization of another deformation band adjacent to the first one. The grain size distribution in the deformation band is extremely unsorted, whereas in the surrounding host rock the grain size distribution can be very well-sorted. These observations appear to contradict the DEM result that indicates granular aggregates with unsorted grain size distributions can deform at lower stresses than granular aggregates with well-sorted grain size distributions. However, this contradiction is only apparent: deformation bands that have formed in high-porosity sandstones (~0.20) have a porosity that is one order of magnitude smaller (0.01–0.02) than in the surrounding host rock (Antonellini *et al.* 1994, Antonellini & Aydin 1994). If we compare Fig. 11(a) and Fig. 10(a) it is clear that almost two orders of magnitude greater stresses are required to deform a sample compacted to 0.15 porosity with a poorly sorted grain-size distribution (D = 0.88) compared to a sample with uniform grain-size distribution, but compacted to 0.2 porosity.

In light of these numerical experiments we tentatively conclude that the phenomenon of strain hardening (Rudnicki & Rice 1975) after development of a deformation band in a porous sandstone is not due to the crushing of grains into fragments of different sizes, but rather to the compaction of the granular aggregate to a lower porosity during shearing. However, because the DEM considers grains that are approximated by a circular shape, we cannot assess the effects of the angularity of crushed grains that may also contribute to strain hardening.

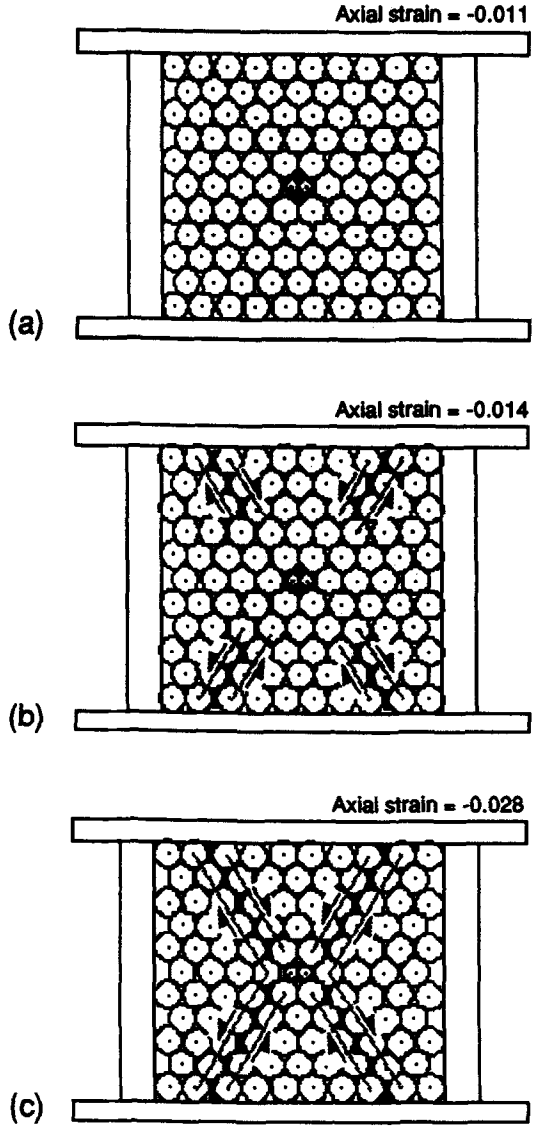

Fig. 13. 'Weak' grain-controlled growth of shear bands. Dilatancy in black. Shear bands are individuated by the shaded lines. The arrows indicate the sense of shear. (a) A weak grain collapses at an axial strain of −0.011. (b) Shear bands propagate from the machine boundaries toward the collapsed grain. (c) Shear bands have completely propagated toward the collapsed grain.

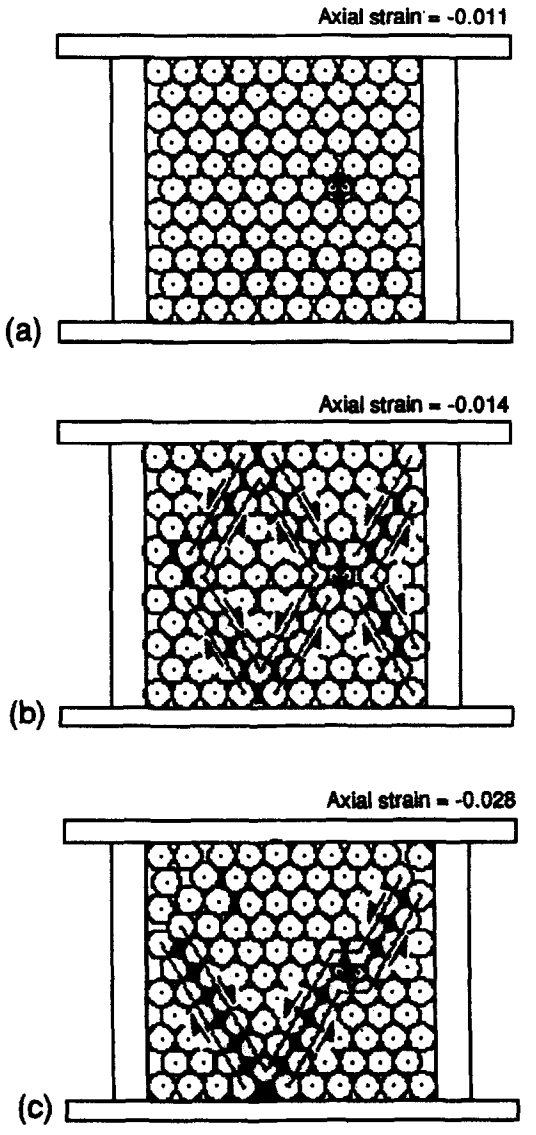

Fig. 14. 'Weak' grain-controlled growth of shear bands. Dilatancy in black. Shear bands are individuated by the shaded lines. The arrows indicate the sense of shear. (a) A weak grain that is shifted to the right respect to the center of the sample collapses at an axial strain of −0.011. (b) Shear bands propagate from the machine boundaries toward the collapsed grain and also in adjacent areas. (c) Two shear bands are fully developed. One of them passes through the collapsed grain.

The nucleation and growth of a shear band in the granular system we investigated starts from an area of local dilatancy and later grows into a fully developed shear band. The importance of dilatancy in geology has been discussed by Mead (1925), and later Frank (1965) pointed out how dilatancy is an important process during faulting and strain localization in a granular medium. More recently Marone & Scholz (1989) have discussed the role of dilatancy in lab experiments on simulated fault gouge. Dilatancy at the grain scale level in a sandstone has been recognized by Antonellini *et al.* (1994) in a microstructural study of deformation bands at Arches National Park. From thin section observations they were able to detect a porosity increase at the tip of a deformation band in a low-porosity sandstone (porosity ~ 9%). The process that they observed is at a grain scale comparable to the numerical experiment shown in Fig. 12.

The position where a deformation band localizes in a sandstone probably depends to some extent on the existence of an area of increased porosity or on the presence of a 'weak' grain that can crush under small contact loads. This scenario is supported by the experiments we have reported here and by lab experiments on loose granular aggregates reported by Desrues (1991). The collapse of the grain has the effect of localizing shear bands at lower loads. It also appears that the position of the 'weak' grain controls where shear bands are going to develop in the sample tested. However the boundaries of our experimental apparatus also play an important role in controlling the nucleating position of the shear bands.

Summarising the results of our numerical study indicate that sorting and initial porosity of the host rock control the mode of deformation within a fault zone in granular material. By modeling the granular materials

with elastic distinct elements, and by performing numerical biaxial experiments on these elements it appears that systems of elements that have a large variability in radius and/or a loose packing (high-porosity) deform at lower applied stresses than systems of elements that have a uniform radius and/or a tight packing (low-porosity). The mode of deformation in the first kind of materials is particulate flow, where elements of different sizes move easily with respect to each other due to a low degree of interlocking. The mode of deformation in the second kind of materials is localized failure on small shear bands. Shear bands in our numerical experiments nucleate as a zone of dilatancy and propagate via organization of dilatant zones into discrete faults; the nucleation and the propagation of a shear band can be controlled by the presence of a flaw in the form of a 'weak grain'.

Acknowledgements—This work has been sponsored by the Rock Fracture Project at Stanford University and by a Phillips Petroleum Company fellowship to M. Antonellini. Thanks to M. Willemse, P. Segall, K. Aziz, G. Mavko and A. Aydin for helpful discussions and to P. Cundall for providing information on the DEM. G. Hirth, D. Scott and J. Evans have provided helpful reviews of this paper.

REFERENCES

Allen, M. D. & Tildesley, D. J. 1987. *Computer Simulation of Liquids*. Clarendon, Oxford.

Anderson, R. S. & Haff, P. K. 1988. Simulation of aeolian saltation. *Science* **241**, 820–823.

Anderson, R. S. & Haff, P. K. 1991. Wind modification and bed response during saltation of sand in air. *Acta Mechanica (suppl.)* **1**, 21–51.

Antonellini, M. A. 1994. Structural and fluid flow properties of faults in porous sandstones. Ph.D. thesis, Stanford University.

Antonellini, M. A. & Aydin, A. 1994. Effect of faulting on fluid flow in porous sandstones: petrophysical properties. *Bull. Am. Ass. Petrol. Geol.* **78**, 355–377.

Antonellini, M. A. & Aydin, A. In press.

Antonellini, M. A., Aydin, A. & Pollard, D. D. 1994. Microstructure of deformation bands in porous sandstones at Arches National Park. *J. Struct. Geol.* **16**, 941–959.

Aydin, A. 1978. Small faults formed as deformation bands in sandstone. *Pure & Appl. Geophys.* **116**, 913–930.

Aydin, A. & Johnson, A. M. 1978. Development of faults as zones of deformation bands and as slip surfaces in sandstone. *Pure & Appl. Geophys.* **116**, 931–942.

Aydin, A. & Johnson, A. M. 1983. Analysis of faulting in porous sandstones. *J. Struct. Geol.* **5**, 19–31.

Bardet, J. P. & Proubet, J. 1992a. The structure of shear bands in idealized granular materials. *Applied Mechanics Review* **45**, S118–S122.

Bardet, J. P. & Proubet, J. 1992b. A numerical investigation of the structure of persistent shear bands in granular media. *Géotechnique* **42**, 599–613.

Bernabe, Y. & Brace, W. F. 1990. Deformation and fracture of Berea Sandstone. In: *The Brittle-Ductile Transition in Rocks* (edited by Duba, A. G., Durham, W. B., Handin, J. W. & Wang, H. F.). *Am. Geophys. Union, Geophys. Monographs* **56**, 91–101.

Biegel, R. L., Sammis, C. G. & Dieterich, J. H. 1989. The frictional properties of a simulated gouge having a fractal particle distribution. *J. Struct. Geol.* **11**, 827–846.

Blenkinsop, T. G. 1991. Cataclasis and processes of particle size reduction. *Pure & Appl. Geophys.* **136**, 59–86.

Borradaile, G. J. 1981. Particulate flow of rock and the formation of cleavage. *Tectonophysics* **72**, 305–321.

Brandt, H. 1955. A study of the speed of sound in porous granular media. *J. appl. Mech.* **22**, 479–486.

Cundall, P. A. 1971. A computer model for simulating progressive, large-scale movements in block rock systems. *Proc. Symp. Int. Soc. Rock Mech., Nancy* **II**, 8.

Cundall, P. A. & Strack, O. D. L. 1979. A discrete numerical model for granular assemblies. *Géotechnique* **29**, 47–65.

Cundall, P. A. 1987. Distinct element models of rock and soil structure. In: *Analytical and Computational Methods in Engineering Rock Mechanics* (edited by Brown, E. T.). Allen & Unwin, London, 129–163.

Cundall, P. A. 1988. Computer simulations of dense sphere assemblies. In: *Micromechanics of Granular Materials* (edited by Satake, M. & Jenkins, J. T.). *Studies Appl. Mech.* **20**, 113–123.

Cundall, P. A. 1989. Numerical experiments on localization in frictional materials. *Ingenieur Archiv.* **59**, 148–159.

Deresiewicz, H. 1958. Mechanics of granular matter. *Advances Appl. Mech.* **5**, 233–306.

Desrues, J. 1991. An introduction to strain localization in granular materials. In: *Physics of Granular Media* (edited by Bideau, D. & Dodds, J.). Nova Science Publishers, New York, 127–143.

Duffy, J. & Mindlin, R. D. 1957. Stress–strain relations and vibrations of a granular medium. *Trans. ASME, J. Appl. Mech.* **25**, 585–593.

Dunn, D. E., LaFountain, L. J. & Jackson, R. E. 1973. Porosity dependence and mechanism of brittle fracture in sandstones. *J. geophys. Res.* **78**, 2403–2417.

Engelder, J. T. 1974. Cataclasis and the generation of fault gouge. *Bull. geol. Soc. Am.* **85**, 1515–1522.

Frank, F. C. 1965. On dilatancy in relation to seismic sources. *Rev. Geophys.* **3**, 485–503.

Gould, H. & Tobochnik, J. 1988. *Computer Simulation Methods, Part I*. Addison-Wesley, Reading, Massachussets.

Haff, P. K. & Anderson, R. S. 1993. Grain scale simulations of loose sedimentary beds: the example of grain-bed impacts in aeolian saltation. *Sedimentology* **40**, 175–198.

Haff, P. K. & Werner, B. T. 1986. Computer simulation of the mechanical sorting of grains. *Powder Technology* **48**, 239–245.

Handin, J., Hager, R. V., Friedman, M. & Feather, J. N. 1963. Experimental deformation of sedimentary rocks under confining pressure: pore pressure effects. *Bull. Am. Ass. Petrol. Geol.* **47**, 717–755.

Hara, G. 1935. Theorie der akustischen Schwingungsausbreitung in gekornten Substanzen und experimentelle Untersuchungen an Kohlepulver. *Elektrische Nachrichten-Technik* **12**, 191–200.

Hertz, H. 1882. Uber die beruhrungfester elastischer Korper. *J. Reine Angew. Math* **92**, 156–171.

Hirth, G. & Tullis, J. 1989. The effects of pressure and porosity on the micromechanics of the brittle-ductile transition in quartzite. *J. geophys. Res.* **94**, 17825–17838.

Hockney, R. W. & Eastwood, J. W. 1989. *Computer Simulation Using Particles*. Adam Hilger, New York.

Jiang, Z. & Haff, P. K. 1993. Multi-particle simulation methods applied to the micromechanics of bedload transport. *Water Resources Research* **29**, 399–412.

Johnson, K. L., 1985. *Contact mechanics*. Cambridge University Press, Cambridge.

Ko, H. Y. & Scott, R. F. 1967. Deformation of sand in hydrostatic compression. *J. Soil Mech. Found. Div. Proc. ASCE* **93**, 137–156.

Lambe, T. W. & Whitman, R. V. 1969. *Soil Mechanics*. Wiley, New York.

Lasek, A. 1992. On some problems of particles behaviour in a shear flow. In: *Sand Transport in Rivers, Estuaries and The Sea* (edited by Soulsby, R. & Bettess, R.). 203–207.

Lemos, J. V., Hart, R. D. & Cundall, P. A. 1985. A generalized distinct element program for modeling jointed rock mass. *Int. Symp. on Fundamentals of Rock Joints*, 335–343.

Maini, T., Cundall, P. A., Marti, J., Beresford, N. L. & Asgian, M. 1978. Computer modeling of jointed rock masses. Technical Report N-78-8, U.S. Army Waterways Experiment Station.

Maklhouf, H. & Stewart, J. J. 1967. Elastic constants of cubical-tetrahedral and tetragonal spheroidal arrays of uniform spheres. *Proc. Int. Symp. on Wave Propagation and Dynamic Properties of Earth Materials*, Albuquerque, New Mexico.

Marone, C. & Scholz, C. H. 1989. Particle-size distribution and microstructures within simulated fault gouge. *J. Struct. Geol.* **11**, 799–814.

Mead, W. J. 1925. The geologic role of dilatancy. *J. Geol.* **33**, 685–698.

Mindlin, R. D. & Deresiewicz, H. 1958. Elastic spheres in contact under varying oblique forces. *Trans. ASME J. Appl. Mech.* **20**, 327–344.

Ng, T. T. & Dobry, R. 1992. A non-linear numerical model for soil mechanics. *Int. J. Num. Analy. Meth. Geomechs* **16**, 247–263.

Rowe, P. W. 1962. The stress–dilatancy relation for static equilibrium of an assembly of particles in contact. *Proc. R. Soc. Lond.* **A269**, 500–527.

Rudnicki, J. W. & Rice, J. R. Theory of inelastic deformation for strain hardening (or softening) materials. *J. Mech. Phys. Solids* **23**, 371–394.

Rutter, E. H. & Hadizadeh, J. 1991. On the influence of porosity on the low-temperature brittle–ductile transition in siliciclastic rocks. *J. Struct. Geol.* **13**, 609–614.

Saltzer, S. D. 1992. Numerical modeling of crustal scale faulting using the distinct and boundary element methods. Ph.D. thesis, Stanford University.

Saltzer, S. D. 1993. Boundary conditions in sandbox models of crustal extension: an analysis using distinct elements. *Tectonophysics* **215**, 349–362.

Saltzer, S. D. & Pollard, D. D. 1992. Distinct element modeling of structures formed during extensional reactivation of basement normal faults. *Tectonics* **11**, 165–174.

Sammis, C., King, G. & Biegel, R. 1987. The kinematics of gouge deformation. *Pure & Appl. Geophys.* **125**, 777–812.

Sammis, C. G. & Biegel, R. 1989. Fractals, fault-gouge, and friction. *Pure & Appl. Geophys.* **131**, 255–271.

Strack, O. D. L. & Cundall, P. A. 1984. Fundamental studies of fabric in granular materials: Interim Report to NSF CEE-8310729. Department of Civil and Mineral Engineering, University of Minnesota, Minneapolis.

Turcotte, D. L. 1992. *Fractals and Chaos in Geology and Geophysics*. Cambridge University Press, Cambridge, U.K.

Werner, B. T. 1987. A physical model of wind-blown sand transport. Ph.D. thesis, California Institute of Technology, Pasadena, California.

Wood, D. M. 1990. *Soil Behaviour and Critical State Soil Mechanics*. Cambridge University Press, Cambridge.

Yin, H., Mavko, G. & Nur, A. 1993. Grain size effects on porosity, permeability and acoustic velocities in granular materials. *Eos* **74**, 568.

Zhang, J., Wong, T. F. & Davis, D. M. 1990. Micromechanics of pressure-induced grain crushing in porous rocks. *J. geophys. Res.* **95**, 341–352.

APPENDIX

Two critical parts of the DEM are the formulation of the force-displacement laws and of the equations governing the motion of the elements. In the following we give the details of our formulation.

Force-displacement laws for elements

The granular medium investigated in our experiments is represented by a system of cylindrical elements ('grains') with radii ranging from 1 to 4 mm and with a length of 25 mm. The length of the cylinders is important to define their mass and is chosen so that the time step in the equations of motion is computationally efficient. Because of the inertia of the system, if the mass of the elements is large enough it is possible to use larger time steps without incurring instability problems. The motion of the elements is caused by the contact forces between elements and by contact forces arising from the movement of the four rectangular blocks that represent an idealized testing machine described in the section on boundary conditions.

The fundamental equations governing the motion of the elements in the DEM are:

$$F = ma \tag{A1a}$$

$$T = I\dot{\omega} \tag{A1b}$$

where F is the net force acting on the element, m is the element mass, and a the linear acceleration of the element. The net force on the element is the sum of the contact forces caused by the surrounding elements and of any body forces (e.g. that due to gravity). Body forces are not considered in our formulation of the DEM as they are insignificant relative to contact forces at the grain scale. The action of the tangential forces due to friction also exerts a torque or moment (T) on the element; this torque is expressed by equation (A1b) where I is the moment of inertia and $\dot{\omega}$ is the angular acceleration. The net torque (T) on the grain is the sum of the many moments caused by tangential forces imparted at contacts with the surrounding elements.

Two contact forces develop: normal forces, F_n, act perpendicular to the tangent line of the contact, and tangential forces, F_s, are parallel to the tangent line of the contact (Fig. A1a). During a single iteration of the program the particles move and overlap (Fig. A1b). The overlap (δ_n) represents the interpenetration between the elements. The time step during each iteration has to be small enough to prevent large unphysical interpenetrations and to provide stability for the system of particles. If the interpenetrations are small relative to the radii of the

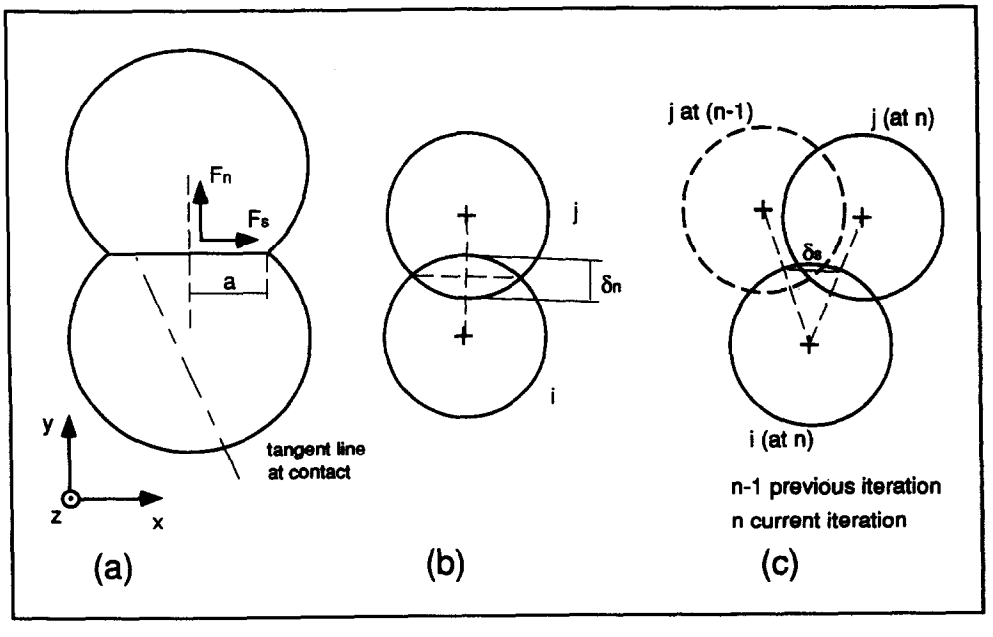

Fig. A1. (a) Elastic Hertzian contact among two spherical grains. a is the half-width of the contact. F_n and F_s are the normal and tangential forces arising during contact between the two grains. Under the action of a normal and a shear loads there are a normal traction distribution and a shear traction distribution along the contact $2a$. (b) Two neighbor elements come in contact. The normal contact force F_n can be calculated from the overlap δ_n between the two elements. (c) The tangential force F_s can be calculated from the displacement δ_s between the points of contact at two successive iterations.

cylinders they can be compared to the elastic deformations at the contact (Fig. A1a), if they are large they cannot be compared to the elastic deformation at the contact and they become unrealistic. According to Cundall (1971) and Haff & Anderson (1993) a suitable time step Δt should meet the requirement:

$$\Delta t \ll \pi\sqrt{\frac{m}{k}} \tag{A2}$$

where m is the mass of an element and k is the stiffness of the contact. The factor π enters this relation from the solution of the differential equation (equation (8) in Haff & Anderson 1993) that is needed to calculate the interpenetration of two grains during a collision; this relation is dependent on the duration of the collision and on the natural frequency of the spring (i.e. the stiffness of the contact). Care must be taken in choosing an appropriate Δt when using elements of different size. To avoid unexpected instability problems, the value of m used in the calculation of Δt should be that of the smallest particle.

The normal contact force is related to the amount of interpenetration measured perpendicular to the tangent line, δ_n (Fig. A1b), via a force-displacement law of the form

$$F_n = K_n\delta_n \tag{A3}$$

where K_n is the normal stiffness of the contact. The usual approach in the DEM is to assume that K_n is constant, but according to Hertz theory (Hertz 1882, Johnson 1985), K_n is related to the half-width a of the contact (Fig. A1a). Following an approach similar to that mentioned by Ng & Dobry (1992) we implemented a force-displacement law that uses a contact stiffness calculated from Hertz theory. According to Hertz (1882) the normal stiffness of two cylinders in contact is:

$$K_n = \frac{\pi G}{(1-\nu)\left[2\ln\left(\frac{4R}{a}\right) - 1\right]} \tag{A4}$$

where G is the elastic shear modulus and ν is Poisson's ratio of the solid. For two solids of revolution the half-width of the contact a in equation (A4) is related to the normal force F_n by the equation (Johnson 1985 p. 93):

$$a = \left(\frac{3F_nR}{4E}\right)^{1/3} \tag{A5}$$

where R is the 'effective' radius of the two solids in contact and E is their Young's modulus. The load F_n at the contact is related to the amount of interpenetration δ_n, and a is a non-linear function of F_n.

Using equation (10) from Johnson (1985 p. 89) it is possible to express the amount of interpenetration between the elements (δ_n) and the half-width of the contact (a) with the relation:

$$a = (2R\delta_n)^{1/2} \tag{A6}$$

where R is the 'effective' radius of the elements in contact, defined by Johnson (1985 p. 92) as:

$$\frac{1}{R} = \frac{1}{R_1} + \frac{1}{R_2}. \tag{A7}$$

In (A7) R_1 and R_2 are the radii of the two solids in contact. Substituting equation (A6) into equation (A4), the normal stiffness in terms of the interpenetration assumes the form:

$$K_n = \frac{\pi G}{(1-\nu)\left[2\ln\left(\left(\frac{8R}{\delta_n}\right)^{1/2}\right) - 1\right]}. \tag{A8}$$

This formulation of the stiffness used in equation (A3) allows one to calculate the reacting force at a contact according to Hertz theory.

When the load between two elements is not applied along their centerline a displacement δ_s arises between distant points in the blocks (Fig. A1c). This tangential displacement is related to the shear contact force F_s. The force-displacement law for the tangential forces that is generally used in the DEM has the form:

$$F_s = K_s\delta_s \tag{A9}$$

where K_s, the shear stiffness of the contact, is a constant. However, Mindlin & Deresiewicz (1958) have shown that slip should be taken into account. Slip, in fact, by dissipating energy introduces non-linearities different from the Hertz non-linearity (Mindlin & Deresiewicz 1958). The changes in stress and displacement caused by a slipping contact depend upon the initial state of loading of the contact and the entire past history of loading. The complete solution to this boundary value problem is given by Mindlin & Deresiewicz (1958).

In our version of the DEM we have not implemented the complete solution that takes slip into account. Rather we have used a simplification that is a linear, normal-force-dependent law. This law uses the initial tangential stiffness given by Mindlin & Deresiewicz (1958) and disregards the history of loading at the contact. The formulation of the contact shear stiffness K_s for two cylinders is

$$K_s = \frac{\pi G a^2}{2R^2(1-\nu)}. \tag{A10}$$

By substituting (A6) into (A10) we obtain:

$$K_s = \frac{\pi G\delta_n}{R(1-\nu)} \tag{A11}$$

and the shear force-displacement law can be calculated using equations (A9) and (A11).

During movement the elements interpenetrate causing shear forces at the contacts. If these forces are very small the elements deform elastically and do not dissipate any energy (energy dissipated by slip is neglected in the DEM), but if they are large there can be some sliding with consequent energy dissipation. At every iteration of the program the tangential force between each element in contact is checked to see if it exceeds the product μF_n, where μ is the coefficient of sliding friction. If $F_s > \mu F_n$ the contact is flagged as 'sliding' and the calculated tangential force F_s is reduced to

$$F_s = \mu F_n. \tag{A12}$$

In this procedure some energy is extracted from the aggregate, thereby contributing to damp the system ('friction damping').

Equations of motion

The motion of each element i is governed by three first-order differential equations

$$F_x(i) = m(i)\frac{\mathrm{d}v_x(i)}{\mathrm{d}t} \tag{A13}$$

$$F_y(i) = m(i)\frac{\mathrm{d}v_y(i)}{\mathrm{d}t} \tag{A14}$$

and

$$\tau_z(i) = I(i)\frac{\mathrm{d}\omega_z(i)}{\mathrm{d}t} \tag{A15}$$

where $F_x(i)$, $F_y(i)$ and $\tau_z(i)$ are the components of the net force and moment acting on the element, $m(i)$ is the mass, $I(i)$ is the moment of inertia, $v_x(i)$, $v_y(i)$ and $\omega_z(i)$ are respectively the components of velocity of the element in the x direction, in the y direction, and the component of angular velocity of the element about the z axis.

The forces and the moment in equations (A13), (A14) and (A15) represent the components of net force and moment exerted on element i by all other elements in contact and by a damping force D_i. The damping force D_i is needed in the DEM, otherwise the elements would vibrate for an infinite time after they start to move because the aggregate is a closed elastic system and any input of energy tends to remain in the system if there is no means of dissipating it. One way of damping the system that has already been mentioned is 'friction damping' (Cundall & Strack 1979). In addition to 'friction damping', in our DEM experiments we have used a viscous or an impact damping scheme. Viscous damping is accommodated by applying a viscous force at the contacts (Cundall 1971, Cundall & Strack 1979). Impact damping is accommodated by applying a force that is able to absorb all the energy due to the initial velocity of the grain (Saltzer 1992).

The physical significance of using one damping method or another is questionable. During deformation of a real granular system, energy is dissipated by friction, grain crushing, plastic deformation, etc. Only the exact quantification of these mechanisms would allow one to devise a damping method that has a meaningful physical significance. As this has not been done, the damping has to be considered simply as an arbitrary means to dissipate energy in order to prevent endless movement of the grains.

By integrating equations (A13), (A14) and (A15) twice, one obtains the equations

$$x(i) = x_0(i) + v_x(i)\Delta t \tag{A16}$$

$$y(i) = y_0(i) + v_y(i)\Delta t \tag{A17}$$

$$\alpha(i) = \alpha_0(i) + \omega_z(i)\Delta t \tag{A18}$$

that give the new coordinates $x(i)$, $y(i)$ of the element's centroid, and the rotation of the particle, $\alpha(i)$, as a function of time, and of the previous position and orientation of the element $(x_0(i), y_0(i), \alpha_0(i))$.

The DEM is computationally intensive, especially when it models many-particle systems and complex interaction laws among the elements. For our numerical simulations we have developed a specific code (Antonellini 1994) to investigate the problem of shear band growth and the development of its microstructure. To limit the time required for the computations we have studied granular systems in which the number of particles ranges from 105 (~40 min CPU time on a SPARC 2 workstation) to 950 (~65 h CPU time). The structure and the listing of the program can be found in Antonellini (1994).